J. Fluid Mech. (2009), *vol.* 628, *pp.* 371–394.
doi:10.1017/S0022112009006296 Printed in the United Kingdom

Combined effects of flow curvature and rotation on uniformly sheared turbulence

D. C. ROACH[1] AND A. G. L. HOLLOWAY[2]†

[1]Department of Engineering, University of New Brunswick, Saint John, New Brunswick E2L 4L5, Canada

[2]Department of Mechanical Engineering, University of New Brunswick Fredericton, New Brunswick E3B 5A3, Canada

(Received 18 March 2008 and in revised form 23 January 2009)

This paper describes an experiment in which a uniformly sheared turbulence was subjected to simultaneous streamwise flow curvature and rotation about the streamwise axis. The distortion of the turbulence is complex but well defined and may serve as a test case for turbulence model development. The uniformly sheared turbulence was developed in a straight wind tunnel and then passed into a curved tunnel section. At the start of the curved section the plane of the mean shear was normal to the plane of curvature so as to create a three-dimensional or 'out of plane' curvature configuration. On entering the curved tunnel, the flow developed a streamwise mean vorticity that rotated the mean shear about the tunnel centreline through approximately 70°, so that the shear was nearly in the plane of curvature and oriented so as to have a stabilizing effect on the turbulence. Hot wire measurements of the mean velocity, mean vorticity, mean rate of strain and Reynolds stress anisotropy development along the wind tunnel centreline are reported. The observed effect of the mean shear rotation on the turbulence was to diminish the shear stress in the plane normal to the plane of curvature while generating non-zero values of the shear stress in the plane of curvature. A rotating frame was identified for which the measured mean velocity field took the form of a simple shear flow. The turbulence anisotropy was transformed to this frame to estimate the effects of frame rotation on the structure of sheared turbulence.

1. Introduction

This paper is the fourth in a series that describes the effects of plane curvature on uniformly sheared turbulence. In all of these experiments the turbulence was developed in a straight wind tunnel section until it was nearly homogeneous and had a self-preserving sheared structure as described by Tavoularis & Karnik (1989). The flow was then passed into a curved wind tunnel section that turned the flow without significantly affecting the uniformity of the shear or the homogeneity of the turbulence but did produce a rotation of the mean shear and substantial adjustments in the anisotropy of the turbulence stress tensor. The previous papers considered plane flow cases: prolonged constant flow curvature (Holloway & Tavoularis 1992), reversing flow curvature (Chebbi, Holloway & Tavoularis 1998) and the combined effects of favourable pressure gradient and flow curvature (Holloway, Roach & Akbary 2005). The present study considered the three-dimensional (or 'out of plane')

† E-mail address for correspondence: holloway@unb.ca

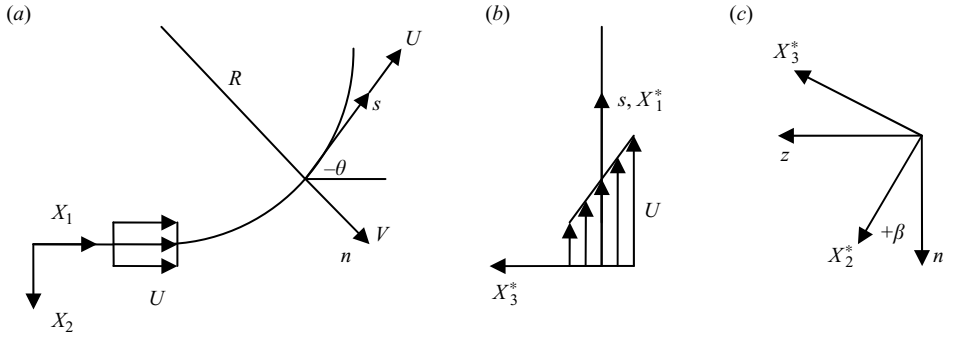

FIGURE 1. Flow configuration and coordinates: (*a*) plane of the curvature showing the *s*, *n* and *z* curvilinear coordinates and the inertial Cartesian coordinates X_i, (*b*) the mean shear (with negative sign) and the rotating coordinates X_i^* and (*c*) rotation of the coordinate system X_i^*, around the streamwise direction by angle β. Note that the mean shear at the start of curvature is in the plane normal to the plane of curvature but by the end of the measurement region in the curved tunnel it has rotated into the plane of curvature.

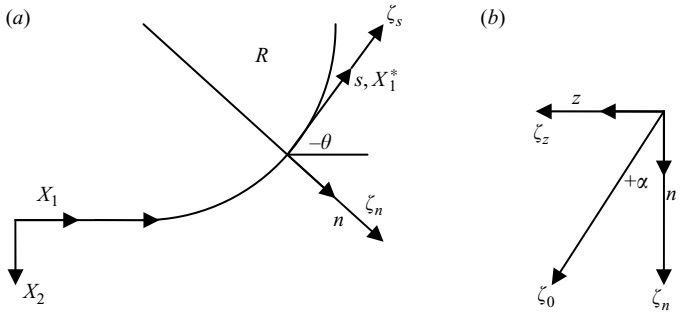

FIGURE 2. (*a*) Components of the mean vorticity ζ in the (s, n, z) coordinate system. (*b*) Projection of the mean vorticity ζ_0 on the cross-flow plane.

case where the mean shear lies in a plane normal to the plane of curvature at the entrance to the curved tunnel as shown in figure 1. A unique feature of this flow was the development of a streamwise component of mean vorticity that rotated the mean shear about the streamwise axis towards the plane of the curvature with the higher mean velocity on the outside of the curve. As a consequence the turbulence was subjected to the combined effects of stabilizing streamwise curvature and rotation about the streamwise axis.

The streamwise mean vorticity ζ_s originates with the vorticity of the mean shear ζ_n present at the start of curvature (see figure 2). As the flow curves this mean vorticity maintains its orientation relative to an inertial frame while being stretched so that it develops a projection on the streamwise direction. The result $\mathrm{d}\zeta_s = 2\ \zeta_n \mathrm{d}\theta$ is generally referred to as Squires Formula (Scorer 1978). Considering the full theory, the streamwise vorticity undergoes a streamwise oscillation with a wavelength of $2\pi\sqrt{UR/\zeta_0}$, where ζ_o is the initial vorticity magnitude. In the present curved flow experiment approximately one-fourth of this period of oscillation was observed.

The turbulence at the start of curvature was typical of sheared flow with one dominant shear stress that transported momentum down the gradient of mean velocity. As the mean shear rotated, two additional shear components of the turbulence stress were generated. The initially dominant shear stress was diminished to nearly

zero. The present paper presents the measured development of both the mean flow and the turbulence anisotropy along the centreline of the curved tunnel section as described above. In addition, an analytical model of the mean vorticity development is presented to assist interpretation of this complex mean flow.

The problem of rotating homogeneous shear flow has received considerable theoretical study because it is conceptually simple and yet retains the essential elements of energy redistribution among both physical directions and scales. Examples of analytical and computational studies are Leuchter, Benoit & Cambon (1992), Salhi and Cambon (1997), Brethouwer (2005), Akylas, Kassinos & Langer (2006) and Jacobitz *et al.* (2008). In each of these cases the axis of mean rotation was normal to the plane of distortion (mean shearing) and the initial state of the turbulence was isotropic with the strength of rotation measured as $\mathscr{R}$ =(twice the frame rotation rate/mean shear rate). In this configuration there is only one non-zero turbulent shear stress due to the statistical symmetry about the plane of shearing. Jacobitz *et al.* (2008) considered very strong rotation with $\mathscr{R} = \pm 0.5, \pm 5$, Akylas *et al.* (2006) considered the case of zero rotation with respect to an inertial frame $\mathscr{R} = -1$, Brethouwer (2005) and Salhi & Cambon (1997) reported studies of $\mathscr{R} = -3/2, -1, -1/2, 0, 1/2$ and Leuchter *et al.* (1992) considered the case of $\mathscr{R} = 2$. In summary, the analysis showed stabilizing effects of rotation for $\mathscr{R} > 0$ and destabilizing effects of rotation for $-1 < \mathscr{R} < 0$ with the maximum instability at $\mathscr{R} = -1/2$. A significant result of these analyses was an understanding of the effects of frame rotation on the pressure strain rate covariance. Computational studies of rotation effects were completed for 5–15 units of shear strain, depending on the rate of rotation, and these provided some qualitative confirmation to the analytical results. Leuchter *et al.* (1992) also presented experimental data for the case with $\mathscr{R} = 2$ for a full 360° of rotation of the plane strain rate direction. This experiment used a rotating grid to generate turbulence that was then passed into a wind tunnel test section whose cross-section imposed plane strain normal to the streamwise direction and hence normal to the axis of rotation. The turbulent kinetic energy at first decayed rapidly and then remained nearly constant while the components of the Reynolds stress anisotropy were observed to oscillate as predicted by theoretical analysis.

There does not appear to be any computational or experimental studies of homogeneous shear flow subjected to rotation about the streamwise or transverse axes. However a comprehensive analytical and numerical study of fully developed channel flow with streamwise rotation was reported by Oberlack *et al.* (2006) for rotation numbers, $Rn = \Omega_s h/u_\tau = 2.5$, 6.5 and 10, where h is the channel width and u_τ is the friction velocity. For the $Rn = 10$ case strong secondary mean flows were observed and all three shear components of the Reynolds stress took on non-zero values with those in the spanwise and transverse planes being the most significant.

An analogy can be made between these rotating homogeneous shear flows and homogeneous curved shear flow. This can be done by equating the frame rotation rate to the rate of rotation of the streamwise direction in the curved flow $\Omega = U/R$. The mean shear rate of the curved flow in this rotating frame is $\partial U/\partial n - U/R$, where n is the coordinate normal to the streamline, so that by analogy we have $\mathscr{R} = 2S/(1-S)$ where $S = (U/R)/(\partial U/\partial n)$. Holloway & Tavoularis (1992) studied uniformly sheared turbulence subjected to prolonged constant curvature experimentally for a range of curvature effects: $-0.5 < S < 0.5$ which corresponds to $-2.4 < \mathscr{R} < 2.0$. These flows were realized using tunnels of two different curvatures in conjunction with five different shear rates (each having a positive and negative sense) to produce 20 flows. For the more strongly curved flows the mean shear was turned up to 40° within the range

of measurement. The more highly sheared cases were subjected to approximately 10 units of shear strain after the imposition of curvature. A significant difference between this experimental study and the rotating shear flow studies cited above was that the turbulence in this flow had growing integral length scales and turbulence stresses that were strongly anisotropic prior to the application of curvature. This was achieved by applying at least 10 units of shear strain in a straight wind tunnel section. Correlations for the exponent of turbulence energy growth, the shear stress anisotropy and the pressure strain rate covariance in terms of the curvature parameter S were presented for the range $-0.2 < S < 0.2$. One of the conclusions of their study was that the turbulence energy decayed for $\mathscr{R} > 0.1$ and grew for $\mathscr{R} < 0.1$. Holloway & Gupta (1993) conducted a computational study of this curved shear flow that was based on Rapid Distortion Theory. Using this method they found that they could predict observed effects of strong curvature such as the reversal of the turbulence shear stress and the scale dependence of curvature effects on the coherence spectrum of the velocity fluctuations.

Considering the present flow as a rotating shear flow the frame rotation would have three components: a component normal to the plane of curvature, $\Omega_z = -U/R$ (as above), a streamwise component Ω_s and a component normal to the plane of the shear. Consequently this flow lacks the symmetries of a flow with the axis of rotation normal to the plane of shearing, and the Reynolds stress tensor potentially has six non-zero components. Nevertheless, the analogy with rotating shear flow will be developed in a detailed way in the next section and used in the discussion of the results.

2. Analytical description of the flow

2.1. *Mean flow*

Figure 1 defines the curvilinear and Cartesian coordinate axes used to describe the present curved shear flow. The s coordinate follows a mean streamline which has a local radius of curvature R. The mean velocity U is tangent to s and the cross-stream mean velocity gradient, subsequently referred to as the mean shear, is uniform. The mean cross-stream velocity components V and W are zero along s but the cross-stream gradients of V and W are not zero. It is assumed that, $\partial V/\partial z + \partial W/\partial n = 0$, which makes the shear strain in the (n, z) plane zero and puts the mean shear entirely in the (s, n) and (s, z) planes. Components of the fluctuating velocity in the (s, n, z) coordinates are designated as u, v and w, respectively. The mean velocity gradient tensor on the mean streamline s for this flow can be expressed in curvilinear coordinates as

$$\nabla \boldsymbol{V} = \frac{1}{2}\begin{pmatrix} 0 & \dfrac{\partial U}{\partial n} - \dfrac{U}{R} & \dfrac{\partial U}{\partial Z} \\ \dfrac{\partial U}{\partial n} - \dfrac{U}{R} & 0 & 0 \\ \dfrac{\partial U}{\partial Z} & 0 & 0 \end{pmatrix} + \frac{1}{2}\begin{pmatrix} 0 & -\zeta_z & \zeta_n \\ \zeta_z & 0 & -\zeta_s \\ -\zeta_n & \zeta_s & 0 \end{pmatrix}. \tag{2.1}$$

The first term represents the mean strain rate and the second the mean vorticity for the simplified flow described above. The mean vorticity components illustrated in figure 2 are defined as

$$\zeta_s = 2\frac{\partial W}{\partial n} \tag{2.2}$$

$$\zeta_n = \frac{\partial U}{\partial z} \tag{2.3}$$

$$\zeta_z = -\left(\frac{\partial U}{\partial n} + \frac{U}{R}\right) \tag{2.4}$$

The resultant vorticity in the (n, z) plane $\zeta_0 = \sqrt{\zeta_n^2 + \zeta_z^2}$ is at the angle $\alpha = \tan^{-1}(\zeta_z/\zeta_n)$ to the n-axis. At the start of curvature the mean shear is in the (s, z) plane and the mean vorticity is directed in the negative n direction. As the flow develops along s the mean vorticity projection ζ_0 swings to the negative z direction so that the plane of mean shear approaches the plane of mean flow curvature with the mean velocity increasing outward from the centre of curvature.

It is possible to define a coordinate system in which (2.1) reduces to a simple shear flow with the streamwise direction X_1^* tangent to s and the transverse direction X_3^* in the plane of the mean shear at all positions along s. The required rotation around the X_1^*axis is

$$\beta = \tan^{-1}\left(\tan\alpha + 2\frac{U}{R}\zeta_n^{-1}\right). \tag{2.5}$$

The magnitude of the resulting mean shear rate is

$$\Sigma = \sqrt{\left(\frac{\partial U}{\partial n} - \frac{U}{R}\right)^2 + \left(\frac{\partial U}{\partial z}\right)^2}. \tag{2.6}$$

Transformation of the velocity components from curvilinear coordinates $(U, V, W)^{\mathrm{T}}$ to U_i^* can be accomplished by the rotational transformation (Hinze 1975)

$$\begin{bmatrix} U_1^* \\ U_2^* \\ U_3^* \end{bmatrix} = \begin{bmatrix} 1 & 0 & 0 \\ 0 & \cos\beta & -\sin\beta \\ 0 & \sin\beta & \cos\beta \end{bmatrix} \begin{bmatrix} U \\ V \\ W \end{bmatrix} \tag{2.7}$$

where the rotation matrix will be referred to as e_{ij}^*.

The velocity components in the inertial Cartesian coordinates U_i can be transformed to the velocity in the shear frame axes U_i^* by a rotation about the X_3 (or equivalently z coordinate) by the angle $-\theta = \int_0^s (1/R)\mathrm{d}s'$, followed by a rotation β about the X_1^* axis to give $U_i^* = U_k e_{kl} e_{li}^*$. The rotation matrix e_{ij} is

$$e_{ij} = \begin{bmatrix} \cos\theta & \sin\theta & 0 \\ -\sin\theta & \cos\theta & 0 \\ 0 & 0 & 1 \end{bmatrix}. \tag{2.8}$$

The resulting rotation rate of the coordinates X_i^* relative to inertial coordinates X_i and expressed in rotating X_i^* coordinates is (Meirovitch 1970)

$$\Omega_i^* = (\dot\beta - \dot\theta\cos\beta,\ \dot\theta\sin\beta,\ \ \dot\theta\cos\beta). \tag{2.9}$$

2.2. *Streamwise deceleration*

The measurements of the mean flow demonstrated a small amount of streamwise strain, $\partial U/\partial s$, and in this section we explore the effects it had on the mean strain rate. The equation of mean flow continuity expressed in X_i^* coordinates gives the cross-plane dilation as

$$\Theta = \frac{\partial U_2^*}{\partial X_2^*} + \frac{\partial U_3^*}{\partial X_3^*}. \tag{2.10}$$

In the present flow, Θ/Σ is small over most of the curved tunnel section but rises near the end to values of 0.15 where it will be shown to have a significant effect on the turbulence. The mean strain rate tensor can be written in the following form in

the rotating X_i^* coordinates:

$$\boldsymbol{S}^* = \frac{1}{2}\begin{pmatrix} -2\Theta & 0 & \Sigma \\ 0 & 2\lambda\Theta & 0 \\ \Sigma & 0 & 2(1-\lambda)\Theta \end{pmatrix}, \tag{2.11}$$

where $\lambda = 0$, $1/2$ or 1 depending on whether the dilation is transverse, axisymmetric or spanwise, respectively. In the presence of mean flow dilation the flow cannot be considered a pure shear flow relative to X_i^* coordinates.

2.3. *Development of the mean vorticity field*

In this section we present an analytical model of the mean vorticity development. It is not meant to be quantitatively accurate but rather to provide some insight into the development of this complex mean flow which is otherwise difficult to understand. To simplify the analysis we will assume axisymmetric dilation ($\lambda = 1/2$). The equations for vorticity development along a streamline in an inviscid flow are (Roach 2001)

$$\frac{U_0}{k}\frac{\mathrm{d}\zeta_s}{\mathrm{d}s} = -2\dot{\theta}\zeta_n - \Theta\zeta_s \tag{2.12}$$

$$\frac{U_0}{k}\frac{\mathrm{d}\zeta_n}{\mathrm{d}s} = -\frac{\zeta_z\zeta_s}{2} + \frac{\Theta}{2}\zeta_s \tag{2.13}$$

$$\frac{U_0}{k}\frac{\mathrm{d}\zeta_z}{\mathrm{d}s} = \frac{\zeta_n\zeta_s}{2} + \frac{\Theta}{2}\zeta_z \tag{2.14}$$

where $k = U_0/U$ and U_0 is the mean speed at the start of curvature. We will associate ζ with the mean vorticity in spite of the fact that the flow is turbulent. This approximation is not as severe as it might first seem because near the tunnel centreline the turbulence is approximately homogeneous and therefore provides minimal net transport of mean vorticity. Equations (2.12)–(2.14) have an exact solution in the form

$$\zeta_s = \frac{U_0}{k}\frac{\mathrm{d}\alpha}{\mathrm{d}s} \tag{2.15}$$

$$\zeta_n = \sqrt{k}\zeta_0\cos\alpha \tag{2.16}$$

$$\zeta_z = \sqrt{k}\zeta_0\sin\alpha \tag{2.17}$$

where ζ_0 is the mean vorticity magnitude at the start of curvature. The angle α of the projection, $\zeta_0 = \sqrt{\zeta_n^2 + \zeta_z^2}$, to the n axis (see figure 2) is determined by the equation

$$\frac{\mathrm{d}^2\alpha}{\mathrm{d}s^2} + \frac{k^{3/2}\zeta_0}{U_0 R}\sin\alpha = 0 \tag{2.18}$$

which has as its solution oscillations analogous to pendular motion with the direction of ζ_0 and the magnitude of the streamwise component of vorticity oscillating along the streamline. In the case of zero dilation, $k = 1$, we can see that the magnitude of ζ_0 remains constant and is equal to the mean shear at the start of curvature.

In the presence of flow dilation $k = 1 + \int_0^s (\Theta/U_0)\mathrm{d}s' > 1$ and there is an increase in ζ_0 at the expense of ζ_s. The present flow parameters are such that only a quarter period of the predicted oscillation is observed and, with $0.9 < k < 1.0$, the effect of dilation on the mean vorticity is mild over most of the tunnel length.

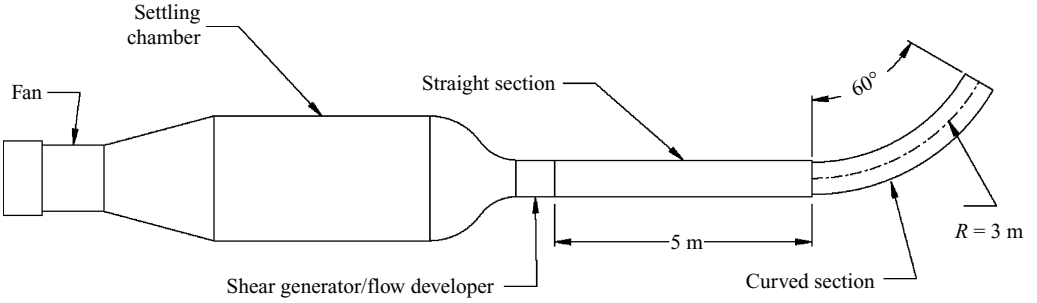

FIGURE 3. Schematic illustration of the wind tunnel showing straight and curved tunnel test sections.

2.4. *Turbulence*

The components of the Reynolds stress tensor in curvilinear coordinates are $\overline{u^2}$, $\overline{v^2}$, $\overline{w^2}$, $\overline{uv}$, $\overline{uw}$ and $\overline{vw}$. The invariant of the Reynolds stress tensor $q^2 = \overline{u^2}+\overline{v^2}+\overline{w^2}$ is twice the turbulent kinetic energy per unit mass. The turbulence parameter of primary interest in this paper is the Reynolds stress anisotropy with components defined as

$$\left.\begin{aligned} m_{uu} &= \frac{\overline{u^2}}{q^2} - \frac{1}{3} \quad m_{vv} = \frac{\overline{v^2}}{q^2} - \frac{1}{3} \quad m_{ww} = \frac{\overline{w^2}}{q^2} - \frac{1}{3} \\ m_{uv} &= \frac{\overline{uv}}{q^2} \quad m_{uw} = \frac{\overline{uw}}{q^2} \quad m_{vw} = \frac{\overline{vw}}{q^2} \end{aligned}\right\} \tag{2.19}$$

In the following presentation and discussion of the results there will be a need to transform the stress anisotropy between the curvilinear coordinates, denoted by m_{uu}, m_{vv}, etc. (referred to as m_{ij}) and the rotating X_i^* coordinates. This can be done using the standard rotational transformation for a second-order tensor (Hinze 1975)

$$m_{ij}^* = m_{kl} e_{ki}^* e_{lj}^* \tag{2.20}$$

where m_{ij}^* is the stress anisotropy tensor in the X_i^* frame.

3. Experimental apparatus and instrumentation

The wind tunnel at the University of New Brunswick is of the open-return type shown in figure 3. The flow is conditioned with a large settling chamber and a 16:1 contraction that produces a flow with a non-uniformity of approximately 1 % and a turbulence intensity of less than 0.1 %. The uniform shear was produced using a shear generator (Tavoularis & Karnik 1989) placed immediately downwind of the nozzle. The wind tunnel and measurement system used in this study are the same as used by Holloway *et al.* (2005) and for further details the reader may consult that paper. The key difference between the previous studies and the present one is that the shear generator was rotated about the streamwise axis by 90° so as to produce a mean shear that lies in a plane normal to the plane of curvature.

The straight tunnel section allows the turbulence to homogenize following the shear generator and to develop a self-preserving structure under the influence of uniform shearing that provides a well-defined initial state of the turbulence for the subsequent application of flow curvature and rotation. Once the flow reaches the end of the straight section, it is passed tangentially into the curved portion of the wind tunnel which had a centreline radius of 3 m and a streamwise length of 3.14 m. The square

Station	1	2	3	4	5	6	7	8	9
s (m)	0.028	0.342	0.656	0.970	1.284	1.598	1.912	2.227	2.541

TABLE 1. Positions of cross-stream measurement planes.

cross-section of the curved tunnel had a dimension of 50 cm, slightly smaller than the straight test section, to facilitate removal of the boundary layers at the entrance of the curved section. In addition the corners of the curved tunnel section were filleted and a slight pressurization of the curved tunnel section was provided to facilitate bleeding of low-speed fluid from the corners. This latter measure caused a gradual deceleration of the flow but prevented flow separation.

Measurements were taken over the wind tunnel cross-section at the nine streamwise locations listed in table 1 so that the cross-stream gradients of the streamwise mean velocity could be adequately assessed. Measurements along the wind tunnel centreline were made at 4 cm intervals in both the straight and curved sections of the tunnel to allow the measurement of the mean velocity and turbulence development. No measurements were made in the last 0.5 m of the curved test section to avoid errors associated with the flow exit. At each position the probe axis was tangent to the tunnel centreline so that strictly speaking the measurements in the curved tunnel corresponded to a coordinate system with a fixed radius of $R' = 3$ m. Here we will present measured quantities, corresponding to the fixed radius of centreline curvature, as being in (s, n, z) coordinates (U, V, m_{uu}, m_{vv}, etc.). The angle between the probe axis and the local mean velocity direction was estimated from the measurements as $\sim V/U$ or $\sim W/U$ and was found to be less than 10° in all cases. This misalignment therefore does not have a significant effect on the accuracy of the hot-wire measurements.

The fluid velocity was measured using standard constant temperature hot-wire anemometry techniques (Tavoularis 2005) and a Dantec P61 X-wire probe. The sensing elements were made from 5 μm diameter tungsten wire, 1.25 mm long and separated by 0.9 mm. Directional calibration of the hot wires for pitch consisted of fitting an effective wire angle to a cosine cooling law. Near the tunnel centreline the angle of the flow to the plane of the wires was at most a few degrees on average and consequently the cooling due to out- of-plane velocities was neglected. Speed calibration of the hot-wires was performed in the wind-tunnel under low-turbulence-flow conditions (shear generator removed) with the probe placed at the first streamwise measurement position. A modified form of King's Law (Roach 2001) was used to correlate the bridge voltages to the flow speed.

The present flow, because of its complex strain history, lacks the symmetry typical of plane shear flows. As a consequence the Reynolds stress tensor had six independent non-zero components $\overline{u^2}$, $\overline{v^2}$, $\overline{w^2}$, $\overline{uv}$, $\overline{uw}$ and $\overline{vw}$. These were measured by a series of rotations of the cross-wire probe about its longitudinal axis. In all, four rotary positions were required: (i) alignment of the cross-wires with the (s, n) plane gave $\overline{u^2}$, $\overline{v^2}$ and $\overline{uv}$, (ii) alignment of the cross-wires with the (s, z) plane gave $\overline{u^2}$, $\overline{w^2}$ and $\overline{uw}$, (iii) alignment of the cross-wires with planes oriented at +45° to the (s, n) plane gives $\overline{u^2}$, $\overline{v'^2}$ and $\overline{uv'}$ where the prime indicates a velocity parallel to the plane of the cross-wires and (iv) rotation of the probe at −45° to the (s, n) plane gives $\overline{u^2}$, $\overline{w''^2}$ and $\overline{uw''}$. The shear stress $\overline{vw}$ was calculated from the difference $\overline{vw} = 1/2(\overline{(v')^2} - \overline{(w'')^2})$. For the details of the procedure see Roach (2001).

Variable	Value	Uncertainty
U ($\mathrm{m\,s^{-1}}$)	10	2 %
V ($\mathrm{m\,s^{-1}}$)	0.5	0.1
W ($\mathrm{m\,s^{-1}}$)	0.5	0.1
ζ_s ($\mathrm{s^{-1}}$)	15	10 %
ζ_n ($\mathrm{s^{-1}}$)	20	10 %
ζ_z ($\mathrm{s^{-1}}$)	20	10 %
Θ ($\mathrm{s^{-1}}$)	3.0	5 %
Σ ($\mathrm{s^{-1}}$)	21	10 %
q^2 ($\mathrm{m^2\,s^{-2}}$)	0.60	3 %
L_{uu} (m)	0.10	15 %
$m_{uu}+1/3$	0.53	4 %
$m_{vv}+1/3$	0.28	8 %
$m_{ww}+1/3$	0.18	8 %
m_{uv}	0.05	0.01
m_{uw}	0.13	0.01
m_{vw}	0.05	0.03

TABLE 2. Systematic and statistical uncertainties of measurement.

The streamwise integral length scale L_{uu} was approximated using temporal integral scales and Taylor's frozen flow approximation. It is not possible to define an integral length scale that is invariant to rotation, as is q^2, when only measurements for streamwise separations are available. However, it should be noted that the streamwise velocity fluctuations and the streamwise separation distance, and hence L_{uu}, are invariant to rotations about the streamwise axis that the mean shear undergoes in the present flow.

Uncertainty in measured quantities was similar to those reported in Chebbi *et al.* (1998) and the results are listed in table 2.

4. Measurements

4.1. *Mean Flow*

The mean shear had components in both the n and z directions that may be inferred from figures 4 and 5. These profiles are representative of the 177 point measurement array used at each of the nine streamwise stations along the curved tunnel to determine the mean shear and the mean vorticity of the flow. At the start of curvature the mean shear is almost entirely in the (s, z) plane and is very uniform as shown in figure 4(a). The mean velocity profile in the (s, n) plane (figure 5a), shows no appreciable shear in the vicinity of the tunnel centreline although it has been turned up slightly towards the tunnel walls at the start of curvature to compensate for subsequent flow development. As the flow develops the mean shear is seen to rotate about the streamwise direction so that in the (s, z) plane the shear gradually weakens while in the (s, n) plane it strengthens. Most of this rotation of the mean shear occurs between stations 7 and 9 at which point it has almost completely rotated into the (s, n) plane with the velocity increasing outward from the centre of curvature; corresponding to the case of stabilizing plane curvature. The flow has also decelerated significantly but the uniformity of the mean shear in the n direction at station 9 (after the streamwise rotation) is surprisingly good. The mean velocity profile in the z direction at station 9, however, contains significant non-uniformities outside of $z = \pm 5$ cm. It is likely that

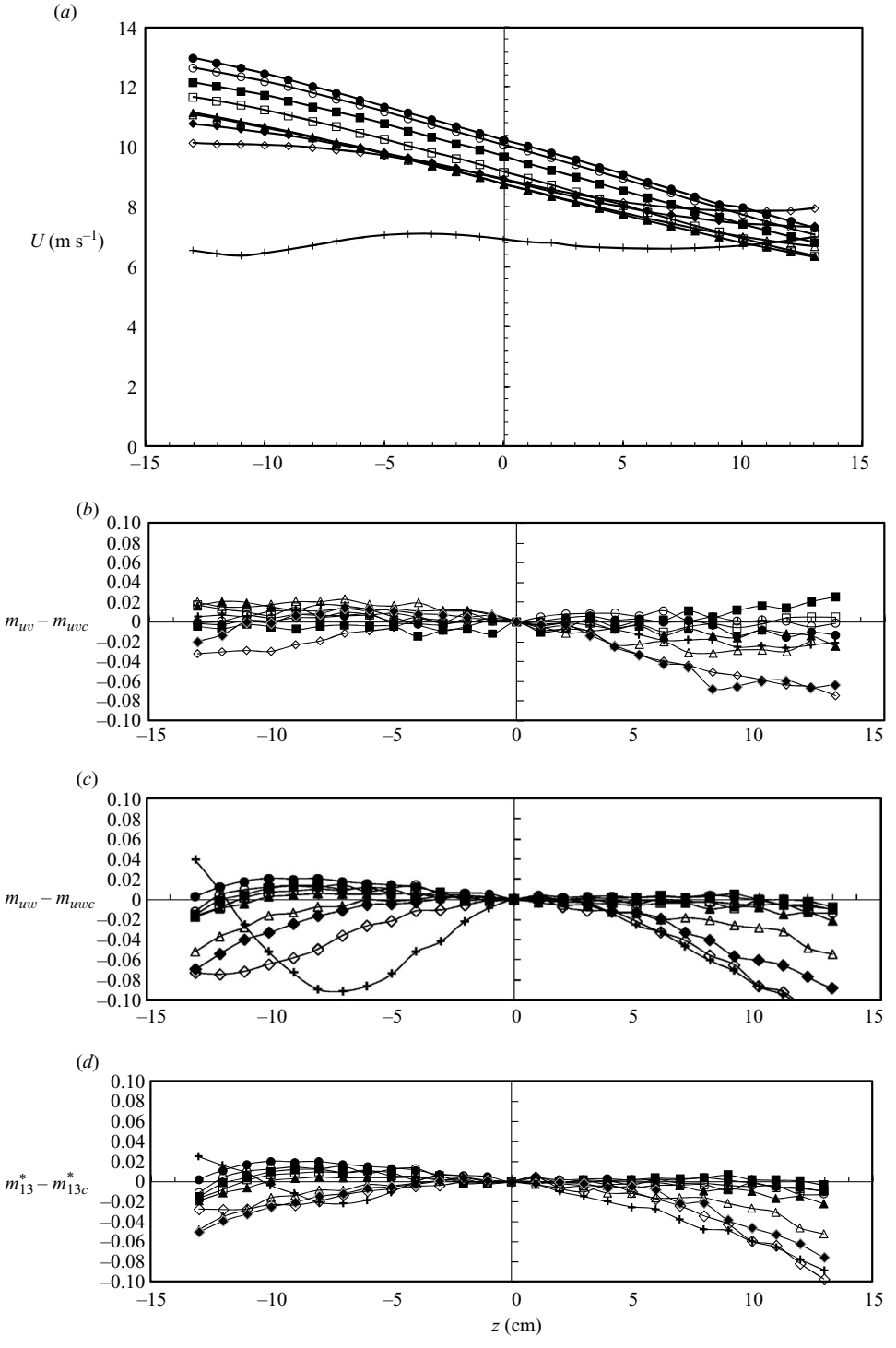

FIGURE 4. Spanwise profiles of the mean streamwise velocity U and the inhomogeneity of the primary shear components of anisotropy m_{uv}, m_{uw} and m^*_{13}, measured at the nine streamwise stations listed in table 1. Symbols denote data from stations: 1 ●, 2 ○, 3 ■, 4 □, 5 ▲, 6 △, 7◆, 8 ◇, 9+.

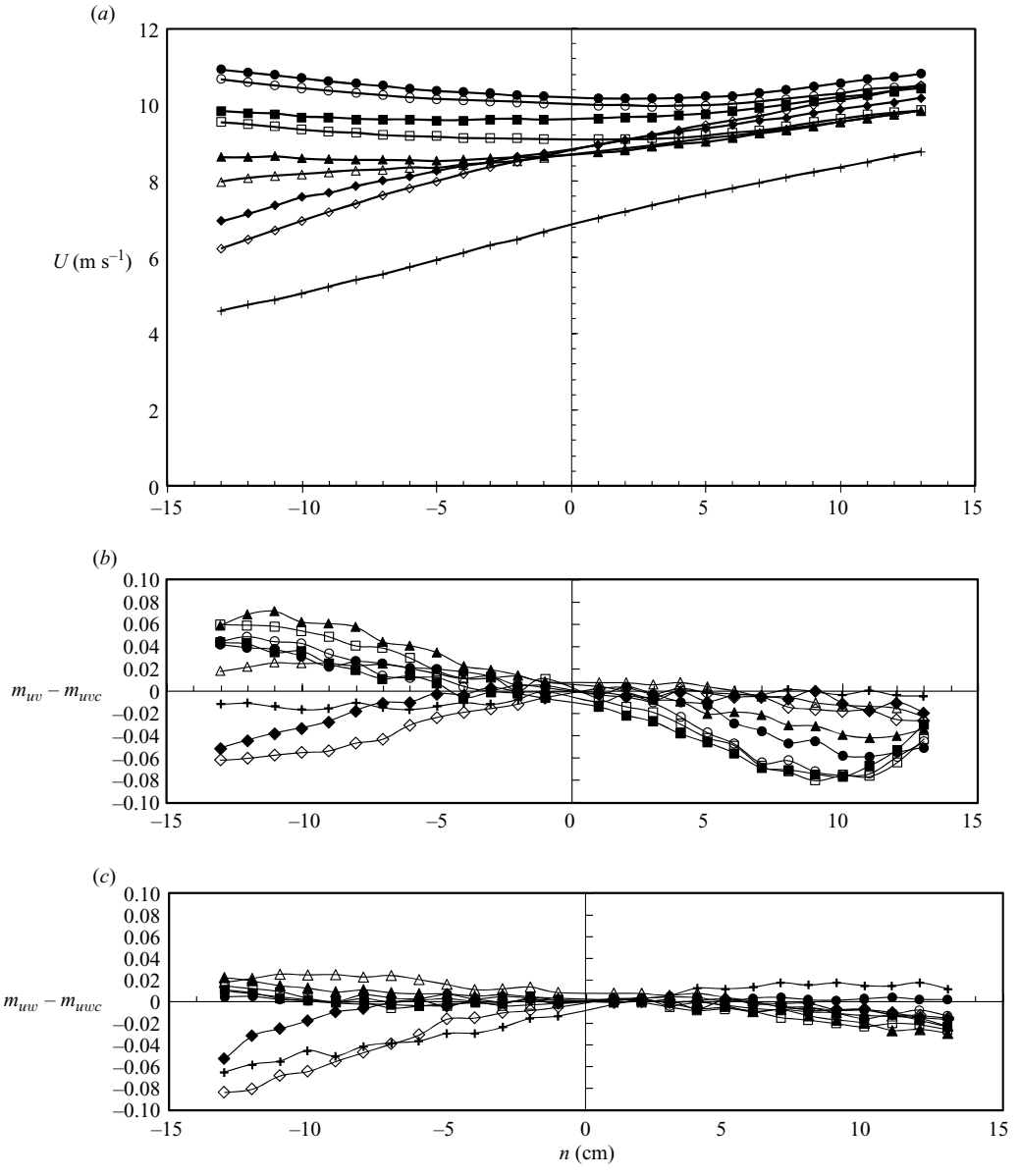

FIGURE 5. Transverse profiles of the mean streamwise velocity U and the inhomogeneity of the primary shear components of anisotropy m_{uv} and m_{uw} measured at the nine streamwise stations listed in table 1. Symbols denote data from stations: 1 ●, 2 ○, 3 ■, 4 □, 5 ▲, 6 △, 7◆, 8 ◇, 9 +.

these non-uniformities are a consequence of the rotation and deceleration of the uniform shear and cannot be reduced.

The inhomogeneous portion of the primary shear components of the turbulence anisotropy, defined as $m_{uv} - m_{uvc}$ and $m_{uw} - m_{uwc}$ where m_{uwc} is the centreline value, are shown in figures 4 and 5. Overall the inhomogeneities of the turbulence in this flow are comparable to previous studies and can be traced to non-uniformities in the slope of the mean velocity profiles and the parameter U/R across the flow.

However, the present flow has unique requirements for the homogeneity that relate to its three-dimensional character. Primarily, it is the fact that what is initially the out-of-plane shear component of anisotropy m_{uv} at station 1 is important for the development of the flow. In plane shear flows, the out-of-plane component of shear anisotropy is nearly zero, due to flow symmetry, and in practice is uncoupled from the mean shear, and mild inhomogeneities are not a serious concern. A similar situation occurs at station 9 for m_{uw} where the mean shear has rotated from the (s, z) plane to the (s, n) plane and it becomes the out-of-plane shear component. Here, in the absence of a strong mean shear, m_{uw} develops inhomogeneities due to the non-uniformities in the mean velocity profile shown in figure 4(a). Conversely, at station 9 we have the inhomogeneity of m_{uv} decreasing since the mean shear is now in the (s, n) plane. A better evaluation of the inhomogeneity of the turbulence can be made by considering the shear component of the anisotropy in the plane of the rotating mean shear $m^*_{13} - m^*_{13c}$ shown in figure 4(d). Here we see that the turbulence has a homogeneity comparable to previous uniformly sheared turbulence studies in the range of $z = \pm 5$ cm and $n = \pm 5$ cm.

The development of the mean velocity U, the total rate of shearing Σ and the dilation Θ are shown in figure 6. There is an increase in centreline mean velocity at the entrance of the curved tunnel followed by a gradual decrease along the length of the curved section. The magnitude of the mean shear rate follows a similar trend. This is to be expected since an invariant of uniformly sheared turbulence is the shear generator constant $k_s = \Sigma/U$ (Tavoularis & Karnik 1989). In the present experiment $k_s = 2.3 \pm 0.1\,\mathrm{m}^{-1}$ both in the straight and curved tunnel sections. The streamwise gradient of the streamwise component of mean velocity was used to calculate the dilation. It is relatively small until the final third of tunnel where it approaches 15 % of the mean shear. It was not possible to estimate the cross-stream mean velocity gradient $\partial V/\partial n$ because its small size was below the measurement uncertainty. This made it impossible to determine by direct measurement whether the dilation in the cross-flow plane is more planar than axisymmetric.

Although the mean streamlines ran very close to the tunnel centreline the local mean streamline curvature, $\kappa = R^{-1} \neq (1/3)\ \mathrm{m}^{-1}$ near the entrance of the curved test section because of the need for a smooth transition from the straight tunnel to the curved tunnel. The actual development of the streamline curvature in this region was estimated from the measurements using the following approximation to the tangential angle $-\theta$ defined in figure 1

$$-\theta = \frac{s}{R'} - \delta \tag{4.1}$$

in which the centreline radius $R' = 3$ m and $\delta = \tan^{-1}(V/U) > 0$. An inherent assumption in the use of (4.1) is that the turbulence and mean distortions are nearly homogeneous near the tunnel centreline. The rate of turning of the streamwise direction is $-\dot{\theta} = U\kappa$ and this has also been plotted in figure 6. In the latter half of the curved tunnel the deviation of the local mean flow direction from the tunnel centreline arises from differences in boundary layer development on the tunnel walls that can produce slight displacements of the mean shear and the centre of mean flow rotation in the cross-flow plane. The components of mean vorticity and stress anisotropy in coordinates tangent to the local flow direction were estimated from the measured components by rotation of the measured quantities about the z axis using the rotation tensor e_{ij}, defined by (2.8), and the angle δ. The adjusted values, shown in figures 7 and 10 as crosses, should be regarded as very approximate.

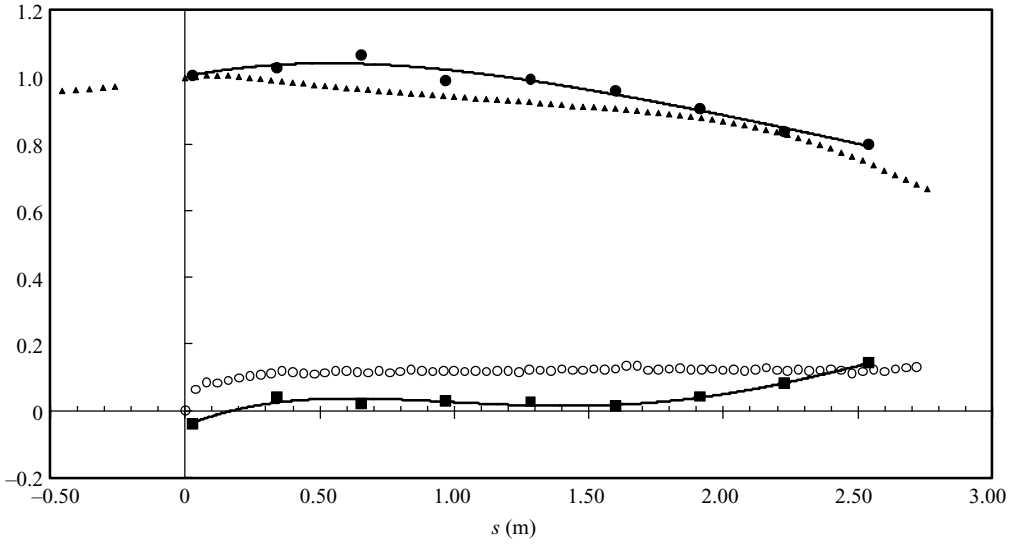

FIGURE 6. Development of the normalized streamwise mean velocity ▲ U/U_0; the total mean shear rate ● Σ/Σ_0; the rate of rotation o $\dot{\theta}/\Sigma_0$ and the mean flow dilation ■ Θ/Σ_0; measured along the wind tunnel centreline. $U_0 = 9.8\,\mathrm{m\,s^{-1}}$ and $\Sigma_0 = 21\ \mathrm{s^{-1}}$.

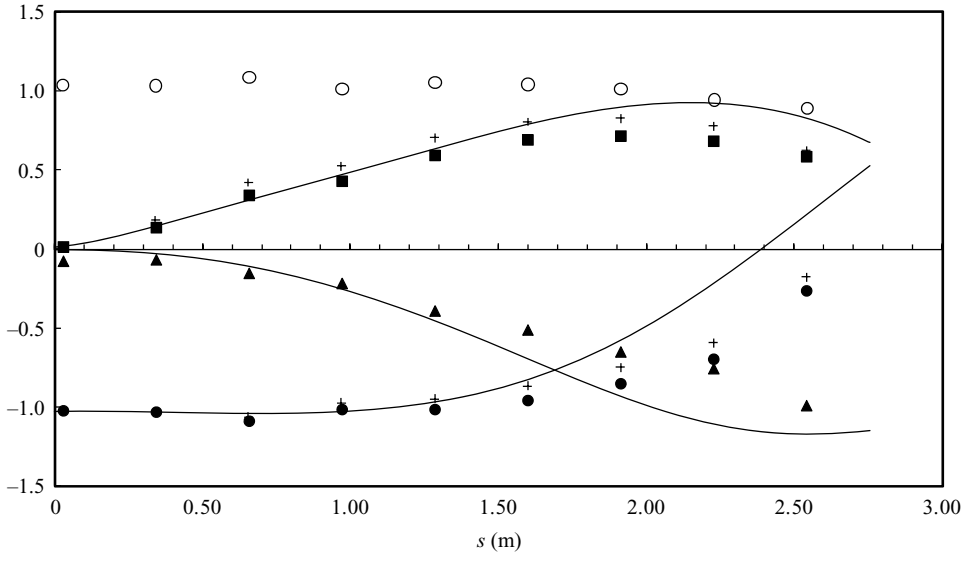

FIGURE 7. Streamwise development of mean vorticity components along the tunnel centreline. Symbols represent measurements of ■ ζ_s/Σ_o, ● ζ_n/Σ_o, ▲ ζ_z/Σ_o, ○ $\sqrt{k}\zeta_0$. Crosses represent an estimate of the vorticity components in coordinates rotated to the local mean flow direction. The solid lines represent the solution of (2.15)–(2.18).

The measured development of the mean vorticity components, ζ_s, ζ_n and ζ_z, is shown in figure 7. Predictions made using (2.15)–(2.18) and the mean flow data of figure 6 are indicated by solid lines. The theory dictates that the streamwise vorticity ζ_s is generated by the turning of the coordinates and stretching of the initial vorticity of the mean shear ζ_n. This development is periodic with the value of ζ_s increasing

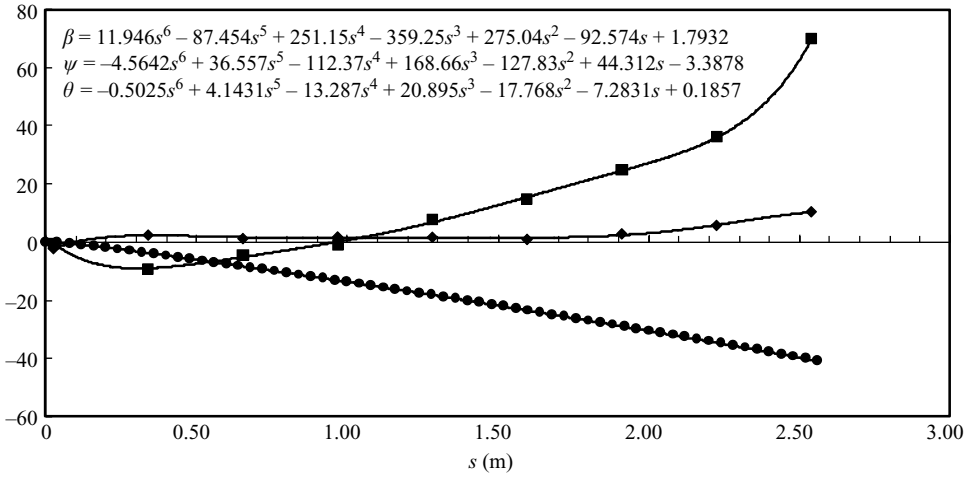

FIGURE 8. Development of the angles of coordinate rotation measured in degrees. Symbols are: ● θ, ■ β and ◆ ψ. The solid lines are sixth-order polynomial curve fits as indicated in the legend.

and then decreasing as the cross-stream components of the mean vorticity ζ_n and ζ_z exchange values in such a way that $\sqrt{k}\zeta_0$ remains constant. The measurements in figure 7 show approximately 1/4 wavelength of the predicted oscillation with the maximum value of the ratio $\zeta_s/\Sigma \sim 0.75$. Considering the errors inherent in the measurement of the mean vorticity components, and the underlying assumption of inviscid flow used in the theory, the agreement between the observed and theoretical values is sufficiently good to accept the theoretical explanation of the observed flow development. As can be seen, even the mean flow has a complex evolution in the present experiment.

The measured development of the angles of mean flow rotation, θ and β is shown in figure 8. The flow curvature turns the streamwise direction, and hence the mean shear, through the angle $\theta \sim -40^\circ$ about the z-axis. The streamwise mean vorticity turns the mean shear through the angle $\beta \sim 70^\circ$ about the streamwise axis X_1^*. The negative values of β during the initial development result from the contribution of curvature (see (2.5)) which begins before the swirling motion. The third angle, shown in figure 8, ψ represents the angle of rotation of the plane of maximum mean shear about the X_2^* axis due to flow dilation. The angle ψ is relatively small but it has been found to be significant as will be described in § 5.

4.2. *Turbulence*

The development of the turbulence scales, $q = \sqrt{q^2}$ and L_{uu}, along the wind tunnel centreline, is shown in figure 9. The turbulence experiences 10 units of shear strain, $\tau = sk$, in the straight wind tunnel prior to the start of curvature and 5 units of shear strain in the curved test section. The velocity and length scales are clearly growing at the end of the straight tunnel and a small portion of this development is included as a reference. After the start of flow curvature the rate of growth of the velocity scale, q, is diminished until q reaches a maximum and begins to decline. The length scale L_{uu} grows at precisely the same rate as q up to $s = 1.50$ m, where the streamwise rotation and flow dilation become significant. An explanation offered for the subsequent decline in L_{uu} is that the negative streamwise strain rate compresses all flow structures, and hence the length scales, in the streamwise direction. As a test of

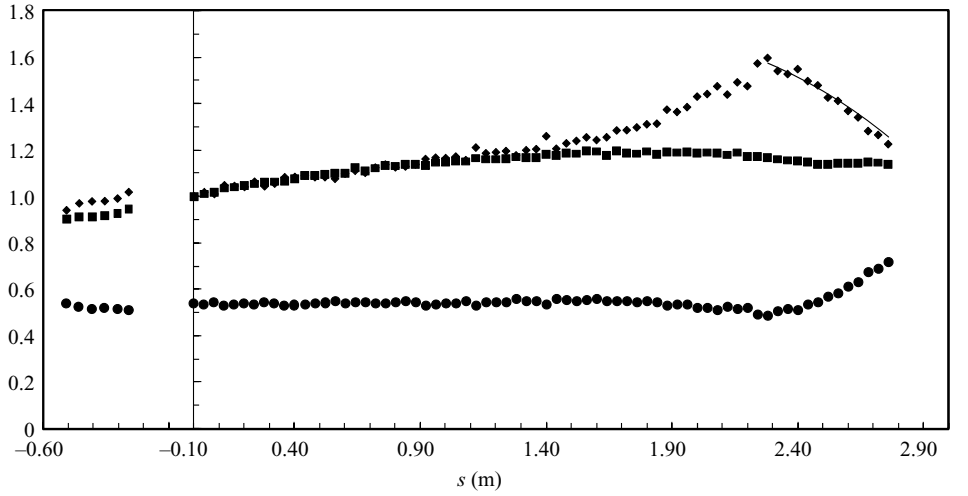

FIGURE 9. Streamwise development of the normalized turbulence scales ■ q/q_o, ◆ L_{uu}/L_{uuo} and ● $q/L_{uu}\Sigma$. The initial values at the start of the curved test section are $q_o = 0.67\,\mathrm{m\,s^{-1}}$ and $L_{uuo} = 6.8\,\mathrm{cm}$. The solid line represents the reduction in length scales expected due to mean streamwise strain alone.

this hypothesis the reduction in length scales due to streamwise strain rate alone was calculated as, $L_{uu} = L_{uu1}\exp(-\int_{s1}^{s}(\Theta/U)\mathrm{d}s'$, with Θ taken from figure 6. The result is shown as the solid line in figure 9. The maximum size reached by the length scale $L_{uu} = 11\,\mathrm{cm}$.

Also plotted in figure 9 is the dimensionless time scale ratio $q/L_{uu}\Sigma$ which compares the eddy turnover rate to the shear rate. It can be seen that $q/L_{uu}\Sigma \sim 0.5$, which is typical of uniformly sheared flows, as far as $s = 2.25\,\mathrm{m}$. Beyond this point the eddy turnover rate appears to be affected by another time scale. It will be shown in § 5 that this other time scale is most likely the streamwise strain rate which is responsible for a significant fraction of the turbulence production in this region.

The dissipation of turbulence kinetic energy ε was not directly measured in this experiment although it is possible to estimate it from the balance of convection and production in uniform shear flow as $\varepsilon = P - U(\mathrm{d}/\mathrm{d}s)(q^2/2)$. In the straight tunnel section prior to the start of curvature, where the shear rate is nearly constant and there are no additional strains, the turbulence energy grows exponentially due to its self-preserving structure and reasonable estimates of $U\mathrm{d}q^2/\mathrm{d}s$ and hence ε can be obtained. In this region of the flow, it was found that $\varepsilon/q^2\Sigma \sim 0.14$ and $\varepsilon/\mathrm{P} \sim 0.64$, both of which are within the range reported by Tavoularis & Karnik (1989). In the curved tunnel section, estimates of ε/P vary from 0.2 near the entrance to 1.5 at $s = 2.52$. It should also be noted that the 'dissipation' of the Reynolds stresses in uniformly sheared laboratory experiments is not isotropic but rather has an anisotropy similar to that of the stresses themselves (Tavoularis & Karnik 1989).

The measured development of the Reynolds stress anisotropy components along the tunnel centreline is shown in figure 10. The three normal components of the stress anisotropy m_{uu}, m_{vv} and m_{ww} remain nearly unaffected until the final third of the tunnel where the streamwise component m_{uu} rises mostly at the expense of m_{vv}. This transfer of energy from the transverse to the streamwise direction begins at $s = 1.60$ m which, according to figure 10, is coincident with the rise in streamwise rotation and the dilation. The dominant shear component of the anisotropy at the

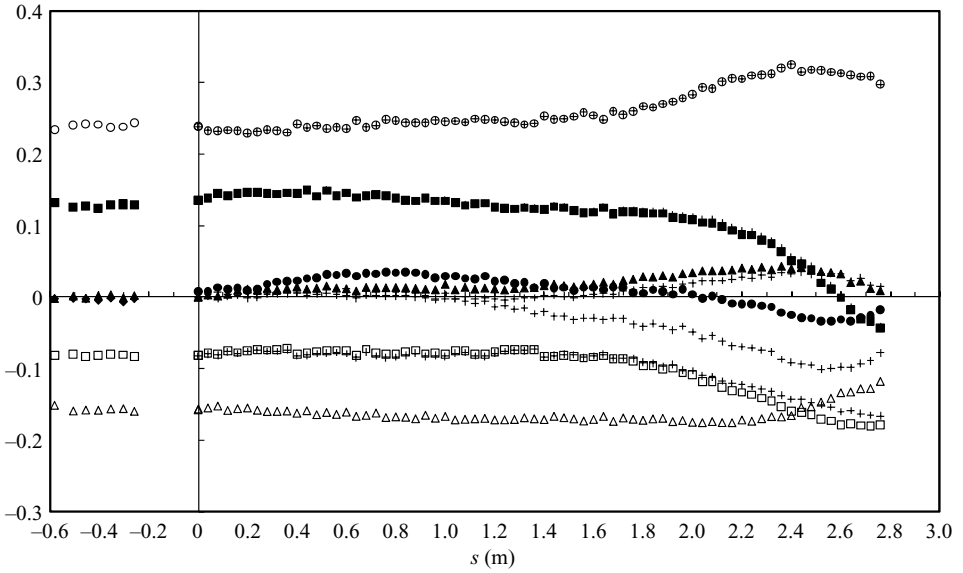

FIGURE 10. Streamwise development of the measured components of the turbulence stress anisotropy along the wind tunnel centreline. Symbols are: ○ m_{uu}, □ m_{vv}, △ m_{ww}, ● m_{uv}, ■ m_{uw}, ▲ m_{vw}. Crosses represent an estimate of the anisotropy components in coordinates rotated to the local mean flow direction.

start of curvature m_{uw} is initially positive, indicating momentum transport down the gradient of mean velocity as one would expect, and declines gradually over most of the tunnel to near zero values. This is consistent with the loss of mean shear in the (s, z) plane shown in figure 6. The development of the shear component of anisotropy m_{vw} remains nearly zero until near the end of the measurement region where it takes small positive values. If it is assumed that there is no mean shear in the (n, z) plane one might suppose that it develops as a result of reorientation of the turbulence. The shear component m_{uv} is initially zero but near the end of the curved tunnel section it develops, presumably with some delay, negative values as one would expect from gradient transport considerations with the mean shear in the (s, n) plane being positive. It is noteworthy that the difference between the measured components of the anisotropy expressed in coordinates tangent to the tunnel centreline and the components transformed to coordinates tangent to the local mean flow direction (indicated by $+$) is small with the single exception of m_{uv}. In this case, the large difference arises from the strong anisotropy of the turbulence according to the transformation $m_{uv}^{+} = -1/2\,(m_{uu} - m_{vv}) \sin\delta + m_{uv} \cos\delta$, but this estimate should be considered more uncertain than the angle δ.

In order to exclude the effects of frame rotation on the turbulence anisotropy we now consider the second invariant of the stress anisotropy tensor

$$II = m_{uu}^2 + m_{vv}^2 + m_{ww}^2 + 2m_{uv}^2 + 2m_{uw}^2 + 2m_{vw}^2. \tag{4.2}$$

This quantity is, by definition, invariant to rotation and has been plotted in figure 11 using the data of figure 10. The value of II shows a similar development to m_{uu} with near constancy up to the final third of the measurement range where the effects of flow rotation and dilation become significant.

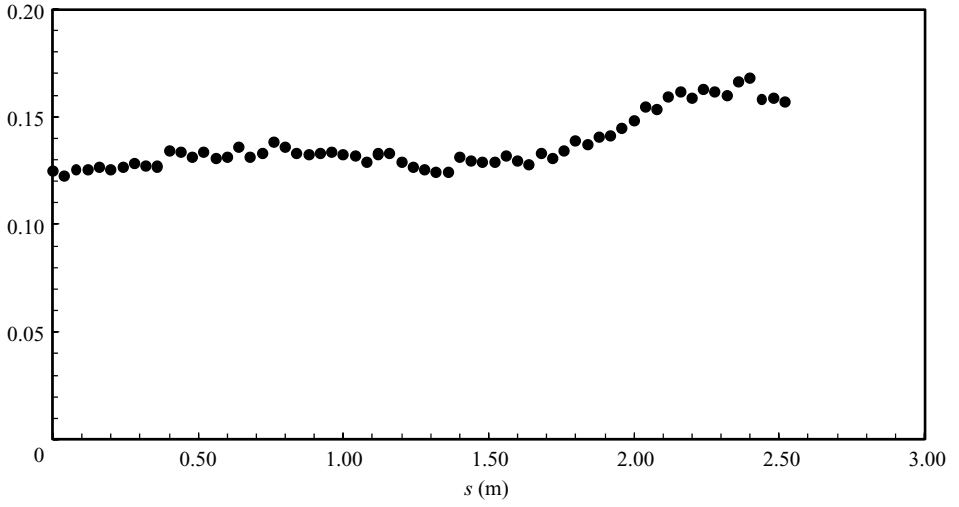

FIGURE 11. The measured development of the second invariant of the Reynolds stress anisotropy tensor *II*.

5. Discussion

The results presented in the previous section show that the mean shear is rotated about the horizontal axis z by the angle θ and about the streamwise axis s by the angle β. The maximum rates of these rotations relative to the mean shearing rate are $-\dot{\theta}/\Sigma \sim 0.15$ and $\dot{\beta}/\Sigma \approx 0.75$, and one would expect significant effects on the turbulence anisotropy to result. In fact, figure 10 shows that m_{uw} is reduced to the point where it changes sign and there is a significant redistribution of energy among the normal components. The shear components m_{uv} and m_{vw} are nearly zero at the start of curvature but reach significant values by the end of the curved section.

In the discussion we explore the effects of the flow rotation on the turbulence as a possible explanation of the observed development of the stress anisotropy shown in figure 10. This will be done by transforming the measured turbulence anisotropy to a frame of reference that rotates with the mean flow. This is done in two steps starting with a transformation of the components of the stress anisotropy to the rotating coordinates, X_i^*. These values are shown in figure 12 and were calculated directly from the anisotropies of figure 10, using the angular data β of figure 8 and the rotational transformation expressed by (2.20). The transformation used has no effect on the streamwise normal component but it does affect the transverse and spanwise normal components as well as the shear components. The changes in all components of the anisotropy are seen to be more modest in this rotating frame than in the laboratory frame but they are still significant. The anisotropy invariant *II*, as indicated by figure 11, is unaffected. Comparing figures 10 and 12 one can conclude that the turbulence is adjusting to the rotation of the mean shear relatively quickly and that it retains its essentially plane shear character. A notable exception is the rise of the shear component, m_{12}^*.

We now consider the effect of streamwise strain rate, and the resulting cross-plane dilation, on the production of q^2 in the rotating coordinates X_i^*

$$\frac{2P}{\Sigma_0 q^2} = -2m_{13}^* \frac{\Sigma}{\Sigma_0} + 2(m_{11}^* - m_{22}^*)\frac{\Theta}{\Sigma_0} \tag{5.1}$$

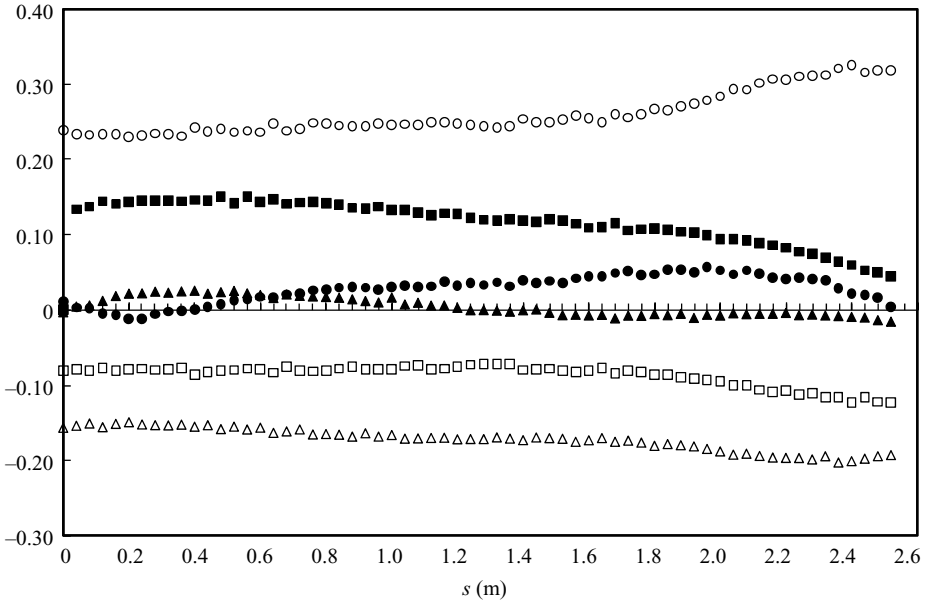

FIGURE 12. Streamwise development of turbulence stress anisotropy transformed to rotating coordinates X_i^*. Values transformed from the anisotropies shown in figure 10 using (2.20). Symbols are: ○ m_{11}^*, □ m_{22}^*, △ m_{33}^*, ● m_{12}^*, ■ m_{13}^*, ▲ m_{23}^*.

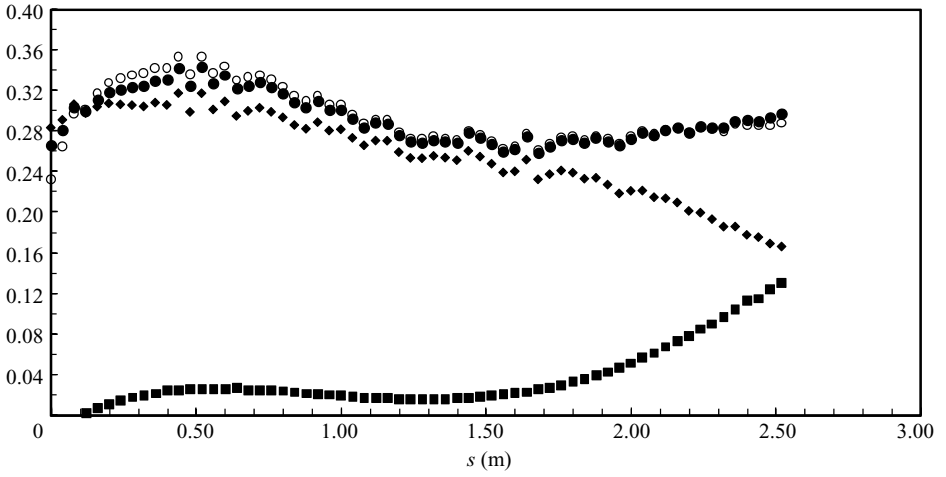

FIGURE 13. Development of normalized production $2P/q^2\Sigma_0$ as defined by (5.1). Symbols are: ● total production, ◆ the production due to shearing alone, ■ production due to streamwise straining alone, ○ the total production according to (5.5).

where it is assumed that the dilation occurs entirely in the plane of the rotating mean shear. The first term on the right-hand side is the normalized production due to shearing and the second is the normalized production due to streamwise straining. Both are proportional to components of the stress anisotropy. These production terms have been plotted separately and as a sum in figure 13.

It is evident that the production due to shear declines steadily over the length of the curved wind tunnel as the dominant shear component m_{13}^* and the shear rate Σ

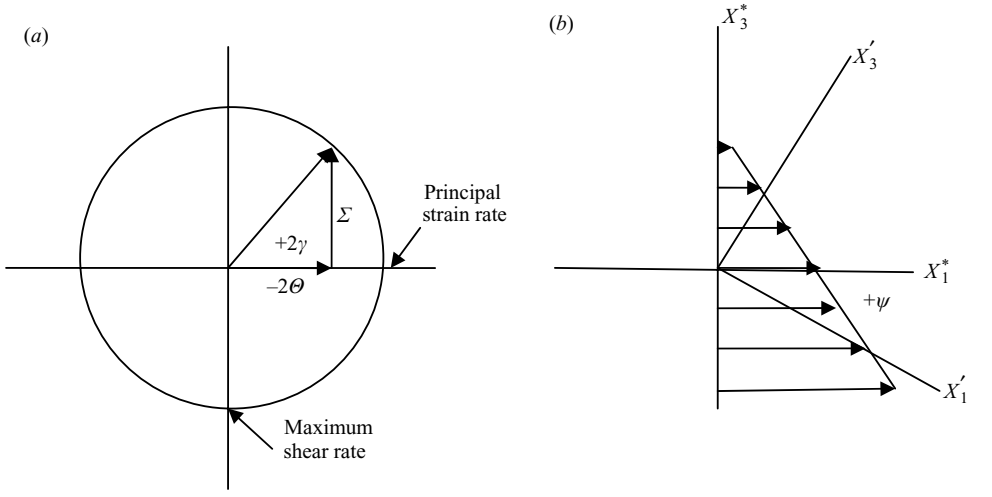

FIGURE 14. Plane of maximum mean shear as determined by streamwise mean strain rate for the case of plane strain. (*a*) Geometric representation of the strain rate transformation to the plane of maximum shear and (*b*) geometric plane showing the Cartesian coordinate directions aligned with the plane of the maximum shear rate.

decline (see figures 6 and 12). The shear component m_{12}^* is not zero but neither does it work against the mean shear and therefore produces no turbulence. The production due to the streamwise strain rate, with $\Theta > 0$, rises to become nearly equal to the shear production by station 9. In fact, it is the streamwise strain rate that maintains the total production, and hence the value of q^2, which remains nearly constant in this portion of the tunnel. The significance of the production due to streamwise strain rate also offers a partial explanation of the rising value of m_{11}^* and falling value of m_{22}^*.

We will now further explain the analogy of the present flow with rotating shear flow by considering the streamwise strain rate from the perspective of its effect on the orientation and magnitude of the maximum mean shear rate as discussed in Holloway *et al.* (2005). For the case of plane dilation, $\lambda = 0$. The principal axis of the mean strain rate with a streamwise stretching, $-\Theta = \partial U_1^*/\partial x_1^* > 0$, and negative shear, $\Sigma = \partial U_1^*/\partial x_3^* < 0$, is shown in figure 14(*a*).

The angle of rotation of the principal strain rate is

$$\gamma = \frac{1}{2}\tan^{-1}(-\Sigma/2\Theta) \tag{5.2}$$

and the rotation of the plane of maximum shear is $\psi = \gamma + \pi/4$. The development of the angle ψ is shown in figure 8. The coordinate parallel to the plane of maximum mean shear will be designated as X_1' as shown in figure 14(*b*). The rotation from X_i^* axes to X_i' requires a rotation about the X_2^* axis using the rotation matrix

$$e_{ij}' = \begin{bmatrix} \cos\psi & 0 & -\sin\psi \\ 0 & 1 & 0 \\ \sin\psi & 0 & \cos\psi \end{bmatrix}. \tag{5.3}$$

The maximum shear rate is increased for both acceleration and deceleration to

$$\Sigma' = \sqrt{4\Theta^2 + \Sigma^2}. \tag{5.4}$$

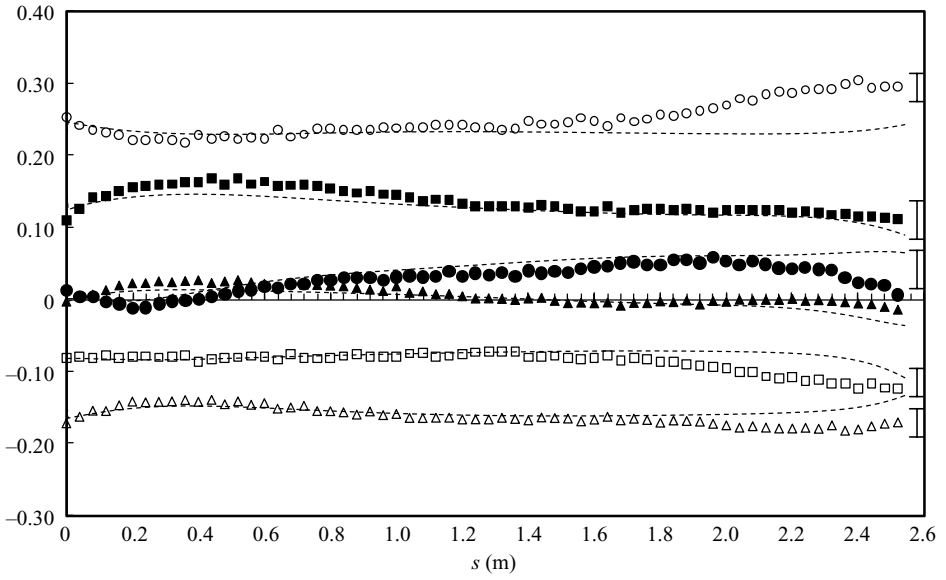

FIGURE 15. Streamwise development of turbulence stress anisotropy in the frame of the rotating mean shear. Values obtained from the anisotropies shown in Figure 12 by transformation using (5.3). Symbols are: ○ m^*_{11}, □ m'_{22}, △ m'_{33}, ● m'_{12}, ■ m'_{13}, ▲ m'_{23}. Dashed lines present the results of model (5.15).

The anisotropy expressed in the axes coincident with the plane of maximum shear (assuming $\lambda = 0$) was calculated from the transformation $m'_{ij} = m^*_{km} e'_{ki} e'_{mj}$ and is shown in figure 15. Also shown in figure 15 are uncertainty bars at station 8 which amount to ± 0.02 for all the normal anisotropy components and ± 0.03 for the shear components. These estimates include the inhomogeneity of the components expressed in (s, n, z) coordinates within ± 5 cm of the centreline. Admittedly these uncertainties are large but they do bound the range of possible effects of the rotation in this flow.

The components of the stress anisotropy viewed in this rotating frame show less variation than those in figures 10 and 12 but the invariant II calculated from all three sets of data is identical as one would expect. Furthermore, the total production of q^2, also an invariant, can be computed as

$$\frac{P}{\Sigma_o q^2} = -2m'_{13}\frac{\Sigma'}{\Sigma_0} \tag{5.5}$$

and this has been added to figure 13. It is nearly identical to that calculated using (4.2).

The largest effects shown in figure 15 are evident in m'_{11}, m'_{22}, m'_{12} and m'_{13} while m'_{33} is practically unchanged. One may conclude from figure 15 that m'_{12} is made positive and m'_{13} is reduced in magnitude by the rotations applied. Oberlack *et al.* (2006) found that streamwise rotation of fully developed channel flow generated significant values of m'_{12}, having the same sign as m'_{13}, and more equal normal stresses. Unfortunately, a direct comparison of streamwise rotation effects between these two flows is hampered by the presence of spanwise and transverse rotations in the present case and the fully developed, inhomogeneous nature of the channel flow.

The analysis of frame rotation effects on a pure shear flow are generally evaluated on the basis of the rates of rotation about the shear frame axis measured relative

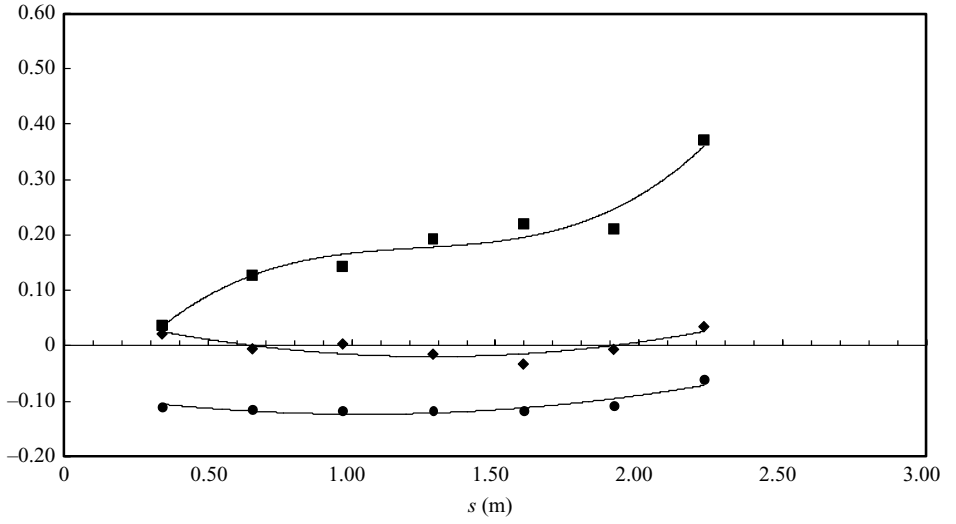

FIGURE 16. Development of the three components of rotation of the frame of the mean shear as calculated from (5.5)–(5.7). Each component is normalized by the magnitude of the shear rate $\Sigma_o = 21\ \mathrm{s}^{-1}$. Symbols are: ■ Ω_1'/Σ_o, ◆ Ω_2'/Σ_o and ● Ω_3'/Σ_o.

to the rate of shearing. The components of this rotation in X_i' coordinates can be expressed for the present flow as (Meirovitch 1970)

$$\Omega_1' = -\cos\beta\sin\psi\dot{\theta} + \cos\psi\dot{\beta} \tag{5.6}$$

$$\Omega_2' = \sin\beta\dot{\theta} + \psi \tag{5.7}$$

$$\Omega_3' = \cos\beta\cos\psi\dot{\theta} + \sin\psi\dot{\beta} \tag{5.8}$$

The rotation rates, Ω_1', Ω_2' and Ω_3', were estimated by fitting sixth-order polynomials to the measured values of θ, β and ψ shown in figure 8. The results, normalized by Σ_o, are shown in figure 16. Of course, considerable caution needs to be exercised when considering these rates of rotation because they include the derivatives of curve fits; however, it seems reasonable to infer that Ω_1' and Ω_3' have opposite signs and both are considerably larger in magnitude than Ω_2'. Equation (5.7) shows that Ω_2' remains small because $\dot{\theta}$ and $\dot{\psi}$ have opposite signs. (Note that uniformly sheared turbulence is very sensitive to spanwise rotation and that a sustained value of $-\Omega_2'/\Sigma' = 0.05$ is sufficient to cause turbulence decay Holloway & Tavoularis 1992.) The total rotation angles around the streamwise axis X_1' and transverse axis X_3' are approximately 1 and 0.5 rad, respectively, in the curved test section.

To assist in explaining the observed effects of rotation on the shear components of the anisotropy demonstrated in figure 15, we first consider the transport equation for the shear components of the Reynolds stresses in a rotating frame (Davidson 2004; Oberlack *et al.* 2006)

$$\frac{\mathrm{d}}{\mathrm{d}t}\overline{u_1'u_3'} + 2\Omega_1'\overline{u_1'u_2'} - 2\Omega_2'\left(\overline{u_1'^2} - \overline{u_3'^2}\right) - 2\Omega_3'\overline{u_2'u_3'} = -\overline{u_3'^2}\Sigma' + \pi_{13} - \varepsilon_{13} \tag{5.9}$$

$$\frac{\mathrm{d}}{\mathrm{d}t}\overline{u_1'u_2'} - 2\Omega_1'\overline{u_1'u_3'} + 2\Omega_2'\overline{u_2'u_3'} + 2\Omega_3'\left(\overline{u_1'^2} - \overline{u_2'^2}\right) = \pi_{12} - \varepsilon_{12} \tag{5.10}$$

$$\frac{\mathrm{d}}{\mathrm{d}t}\overline{u_2'u_3'} + 2\Omega_1'\left(\overline{u_2'^2} - \overline{u_3'^2}\right) - 2\Omega_2'\overline{u_1'u_2'} + 2\Omega_3'\overline{u_1'u_3'} = \pi_{23} - \varepsilon_{23} \tag{5.11}$$

$$\frac{\mathrm{d}}{\mathrm{d}t}\overline{u_1'^2} + 4\Omega_2'\overline{u_1'u_3'} - 4\Omega_3'\overline{u_1'u_2'} = -2\overline{u_1'u_3'}\,\Sigma' + \pi_{11}{}' - \varepsilon_{11} \tag{5.12}$$

$$\frac{\mathrm{d}}{\mathrm{d}t}\overline{u_2'^2} - 4\Omega_1{}'\overline{u_2'u_3'} + 4\Omega_3'\overline{u_1'u_2'} = \pi_{22} - \varepsilon_{22} \tag{5.13}$$

$$\frac{\mathrm{d}}{\mathrm{d}t}\overline{u_3'^2} + 4\Omega_1{}'\overline{u_2'u_3'} - 4\Omega_2'\overline{u_1'u_3'} = \pi_{33} - \varepsilon_{33} \tag{5.14}$$

The left-hand side of (5.9)–(5.14) represents the kinematic effect of frame rotation on the rate of change of the stress components expressed in rotating coordinates. The right-hand side represents the production due to shearing, the pressure strain rate correlation and the 'dissipative' effect on the correlation, respectively. Given the data of figure 15 we can test the *hypothesis* that the pressure–strain rate terms and the dissipative terms of (5.9)–(5.14) do not depend on flow rotation.

In the present flow we have $\overline{u_2'u_3'}$ negligible, $\overline{u_1'u_3'}$ and $\overline{u_1'u_2'}$ positive and $\overline{u_1'^2} > \overline{u_2'^2} > \overline{u_3'^2}$. Considering the explicit rotation terms of (5.9) we see that the sensitivities of $\overline{u_1'u_3'}$ to the three components of rotation would be in the order Ω_2', Ω_1' and Ω_3': Positive values of Ω_1' and negative values of Ω_2' tending to decrease $\overline{u_1'u_3'}$. Now consider the sensitivity of the out-of-plane shear stresses, $\overline{u_1'u_2'}$ and $\overline{u_2'u_3'}$ to rotation. In both (5.10) and (5.11) we see a strong sensitivity to the rotations to Ω_1' and Ω_3'. For (5.10) these terms are additive in the present flow ($\Omega_1' > 0$ and $\Omega_3' < 0$) and tend to make $\overline{u_1'u_2'}$ more positive. In (5.11) explicit rotation terms have opposite signs and nearly cancel for the given state of turbulence stress. These observations are consistent with the data in that $\overline{u_1'u_3'} > \overline{u_1'u_2'} > \overline{u_2'u_3'} \sim 0$. At the least we can conclude that the pressure strain rate and dissipative terms of (5.9)–(5.11) do not completely negate the explicit effects of the rotation. Now considering (5.12)–(5.14) for the normal stresses we find that the most significant term is $-4\Omega_3'\overline{u_1'u_2'}$, which transfers energy from $\overline{u_1'^2}$ to $\overline{u_2'^2}$. The next most significant terms would be $4\Omega'_2\overline{u_1'u_3'}$, which transfers energy from $\overline{u_1'^2}$ to $\overline{u_3'^2}$. The term $-4\Omega'_1\overline{u_2'u_3'}$ is made negligible by the weak correlation between transverse and spanwise fluctuations. These observations are inconsistent with the data so we could conclude that the normal components of the pressure strain rate and dissipative terms at the least negate the explicit effects of frame rotation in the present case.

We next explore the effect of rotation on the development of the stress anisotropy in the present flow using an extension of the model introduced by Holloway & Tavoularis (1998) to explain the effects of plane curvature on sheared turbulence. The model assumes that the development of the stress anisotropy M_{ij} expressed in inertial frame coordinates X_i can be described by the equation

$$\frac{\mathrm{d}M_{ij}}{\mathrm{d}t} = -\left(M_{ij} - M_{kl}^r R_{klij}\right)\Sigma' \tag{5.15}$$

where $\mathrm{d}t = U\mathrm{d}s$, $R_{klij} = e'_{mk}e'_{nl}e^*_{rm}e^*_{sn}e_{ir}e_{js}$ is the rotation tensor which includes the rotations due to $-\psi(t)$, $-\beta(t)$ and $-\theta(t)$, in that order, and

$$M_{kl}^r = \begin{bmatrix} 0.24 & 0 & 0.13 \\ 0 & -0.08 & 0 \\ 0.13 & 0 & -0.16 \end{bmatrix} \tag{5.16}$$

is the anisotropy tensor of a rectilinear shear flow. The values chosen for (5.16) are those just prior to the start of curvature in the present experiment. Equation (5.15) asserts that in the absence of shearing the anisotropy components, assumed to

be non-zero, remain constant in inertial coordinates. In the presence of shearing, the anisotropy in the rotating frame tends towards the anisotropy of rectilinear shear flow, M^r_{kl}, with a time scale equal to the inverse shear rate Σ'^{-1}. Once the integration of (5.15) is complete for the interval of interest the stress anisotropy in the rotating frame is obtained by applying the rotations in the order θ, β and ψ to give $m'_{ij} = M_{kl}\ R_{jilk}$.

Results of applying (5.15) to the present flow using the angle data provided in figure 8 is represented by the dashed lines shown in figure 15. It is apparent that the model results follow the shear components of the anisotropy fairly accurately. In this context the development of positive values of m'_{12} would be ascribed to a delay in the turbulence adjustment to the rotation of the mean shear. On the other hand the model mostly omits the effects of the rotation on the normal stresses, and (not shown) the invariant *II*. Adjusting the time scale used in (5.12) gives only marginal improvement. Consistent with (5.9)–(5.14) this analysis would conclude that the observed changes in the shear components arise largely from rotation of the shear while the effects on the normal stresses result from other dynamic processes. Davidson (2004) discusses the effects of rotation in terms of the Rossby number, $Ro = u'/l\Omega$, and makes the observation for $Ro \leqslant 1$; there are significant changes in the structure of homogeneous turbulence. In the present flow, we have $Ro = q_o/\Omega\ L_{uuo} \sim 1$ at position 8 using $\Omega = \sqrt{\Omega'^2_1 + \Omega'^2_2 + \Omega'^2_3} \sim 8$, $q_o = 0.67\,\mathrm{m\,s^{-1}}$ and $L_{uuo} = 0.068\,\mathrm{m}$. At position 7 the mean rotation lies close to the plane of the shear and at -26° to the X'_1 axis while at position 8 it is at -10°. This direction should be considered relative to the principal axis of mean strain rate which is at an angle of -45° to X'_1.

6. Conclusions

A novel flow in which uniformly sheared turbulence was subjected to plane flow curvature and rotation about the streamwise axis was introduced. At the start of flow curvature the mean shear was in a plane normal to the plane of curvature. This initial condition produced a streamwise mean vorticity that was responsible for the rotation of the shear. The Reynolds stress anisotropy tensor had typical values for uniformly sheared turbulence at the start of curvature but as the flow developed the shear component in the plane normal to the plane of curvature, which is the plane of the mean shear at the start of curvature, decreased substantially while the shear component in the plane of the curvature developed non-zero values. When the turbulence anisotropy was transformed to a frame which rotates with the mean shear it was found that the adjustments due to rotation were more modest and that the turbulence was able to follow the rotating shear closely while retaining its essentially shear character. This result suggests that the observed changes in the turbulence anisotropy relative to laboratory frame results mostly from the rotation of the turbulence relative to these axes.

REFERENCES

Akylas, E., Kassinos, S. C. & Langer, C. A. 2006 An analytical solution for rapidly distorted turbulent shear flow in a rotating frame. *Phys. Fluids* **18**, 085104–1.11.

Brethouwer, G. 2005 The effect of rotation on rapidly sheared homogenous turbulence and passive scalar transport. Linear theory and direct numerical simulation. *J. Fluid Mech.* **542**, 305–342.

Brodkey, R. S. 1967 *The Phenomenon of Fluid Motions*. Addison Wesley.

Chebbi, B., Holloway, A. G. L. & Tavoularis, S. 1998 The response of sheared turbulence to changes in curvature. *J. Fluid Mech.* **358**, 223–244.

Davidson, P. A. 2004 *Turbulence: An Introduction for Scientists and Engineers*. Oxford University Press.

Hinze, J. 1975 *Turbulence*. McGraw-Hill.

Holloway, A. G. L. & Gupta, R. 1993 The influence of linear mechanisms during the adjustment of sheared turbulence to flow curvature. *Phys. Fluids* A **5** (12), 3197–3206.

Holloway, A. G. L., Roach, D. C. & Akbary, H. 2005 Combined effects of favourable pressure gradient and streamline curvature on uniformly sheared turbulence. *J. Fluid Mech.* **526**, 303–336.

Holloway, A. G. L. & Tavoularis, S. 1992 The effects of curvature on sheared turbulence. *J. Fluid Mech.* **237**, 569–603.

Holloway, A. G. L. & Tavoularis, S. 1998 A geometric explanation of the effects of mild streamline curvature on the turbulence anisotropy. *Phys. Fluids* **10**, 1733–1741.

Jacobitz, F. G., Liechtenstein, L., Schneider, K. & Farge, M. 2008 On the structure and dynamics of sheared and rotating turbulence: direct numerical simulation and wavelet-based coherent vortex extraction. *Phys. Fluids* **20**, 045103:1–13.

Leuchter, O., Benoit, J. P. & Cambon, C. 1992 Homogenous turbulence subjected to rotation-dominated plane distortion. In *Proceedings of the Fourth European Turbulence Conference*, Delft, The Netherlands.

Meirovitch, L. 1970 *Methods of Analytical Dynamics*. McGraw-Hill.

Oberlack, M., Cabot, W., Pettersson-Reif, B. A. & Weller, T. 2006 Group analysis, direct numerical simulation and modeling of a turbulent channel flow with streamwise rotation. *J. Fluid Mech.* **562**, 383–403.

Roach, D. C. 2001 Structure of swirling and accelerating turbulent cured shear flows. PhD Thesis, University of New Brunswick.

Salhi, A. & Cambon, C. 1997 An analysis of rotating shear flow using linear theory and DNS and LES results. *J. Fluid Mech.* **347**, 171–195.

Scorer, R. S. 1978 *Environmental Aerodynamics*. John Wiley and Sons.

Tavoularis, S. 2005 *Experiments in Fluid Mechanics*. Cambridge Press.

Tavoularis, S. & Karnik, U. 1989 Further experiments on the evolution of turbulent stresses and scales in uniformly sheared turbulence. *J. Fluid Mech.* **204**, 457–478.